Cell

Structural and Energetic Mechanisms of Cooperative Autoinhibition and Activation of Vav1

Bingke Yu,[1,2,5] Ilídio R.S. Martins,[1,2,3,5] Pilong Li,[1,2] Gaya K. Amarasinghe,[1,2,6] Junko Umetani,[1] Martin E. Fernandez-Zapico,[4] Daniel D. Billadeau,[4] Mischa Machius,[1,7] Diana R. Tomchick,[1] and Michael K. Rosen[1,2,*]

[1]Department of Biochemistry
[2]Howard Hughes Medical Institute
University of Texas Southwestern Medical Center, 5323 Harry Hines Boulevard, Dallas, TX 75390-8816, USA
[3]Departamento de Bioquímica, Faculdade de Ciências e Tecnologia da Universidade de Coimbra, Coimbra 3001-401, Portugal
[4]Department of Immunology and Division of Oncology Research, Schulze Center for Novel Therapeutics, Mayo Clinic, 200 First Street SW, Rochester, MN 55905, USA
[5]These authors contributed equally to this work
[6]Present address: Department of Biochemistry, Biophysics, and Molecular Biology, 4210 Molecular Biology Building, Iowa State University, Ames, IA 50011, USA
[7]Present address: University of North Carolina, School of Medicine, Chapel Hill, NC 27599, USA
*Correspondence: michael.rosen@utsouthwestern.edu
DOI 10.1016/j.cell.2009.12.033

SUMMARY

Vav proteins are guanine nucleotide exchange factors (GEFs) for Rho family GTPases. They control processes including T cell activation, phagocytosis, and migration of normal and transformed cells. We report the structure and biophysical and cellular analyses of the five-domain autoinhibitory element of Vav1. The catalytic Dbl homology (DH) domain of Vav1 is controlled by two energetically coupled processes. The DH active site is directly, but weakly, inhibited by a helix from the adjacent Acidic domain. This core interaction is strengthened 10-fold by contacts of the calponin homology (CH) domain with the Acidic, pleckstrin homology, and DH domains. This construction enables efficient, stepwise relief of autoinhibition: initial phosphorylation events disrupt the modulatory CH contacts, facilitating phosphorylation of the inhibitory helix and consequent GEF activation. Our findings illustrate how the opposing requirements of strong suppression of activity and rapid kinetics of activation can be achieved in multidomain systems.

INTRODUCTION

Vav proteins are guanine nucleotide exchange factors (GEFs) for small GTPases in the Rho family (Bustelo, 2001; Tybulewicz, 2005). They play important roles in actin regulatory pathways in numerous cell types and control diverse processes including immune cell development and activation, neuronal development, and angiogenesis. N-terminal truncations of Vav proteins lead to cell transformation (Katzav et al., 1989), and the wild-type proteins have been implicated in the development and severity of a variety of cancers, including those of the brain, pancreas, and skin (Dong et al., 2006; Katzav, 2007). Vav1 is expressed in hematopoietic cells, where it activates the Rac GTPase in response to Src- and Syk-family kinase signals downstream of the T cell, B cell, and Fcγ receptors. It controls functions such as the antigen response of T cells, phagocytosis by macrophages, and superoxide production by neutrophils (Hall et al., 2006; Tybulewicz, 2005; Utomo et al., 2006). Vav2 and Vav3 are more widely expressed and play similarly important roles in development and cell function throughout the body (Cowan et al., 2005; Sauzeau et al., 2006).

Vav proteins are composed of eight domains: calponin homology (CH), Acidic (Ac), Dbl homology (DH), pleckstrin homology (PH), zinc finger (ZF), Src homology 3 (SH3), Src homology 2 (SH2), and a second SH3. The DH domain catalyzes guanine nucleotide exchange in Rho family GTPases (Abe et al., 1999), and many Vav functions have been ascribed to this activity. The five N-terminal domains (abbreviated CADPZ; other fragments are designated analogously) function together to regulate the biochemical activity of the DH domain; the C-terminal Src homology domains are thought to mediate cellular localization (Figure 1A) (Bustelo, 2001; Tybulewicz, 2005). The GEF activity of Vav1 is autoinhibited by binding of a helix from the C terminus of the Ac domain (residues 167–178) into the active site of the DH domain, blocking access to substrate (Abe et al., 1999; Aghazadeh et al., 2000; Lopez-Lago et al., 2000). This core inhibitory interaction is relieved by phosphorylation of Tyr174 in the inhibitory helix, which melts the helix and displaces it from the DH domain (Aghazadeh et al., 2000; Han et al., 1998). In the cell, Tyr174 is phosphorylated within seconds of receptor stimulation by Src- and Syk-family kinases, rapidly initiating downstream signaling. We recently demonstrated that an Ac-DH fragment

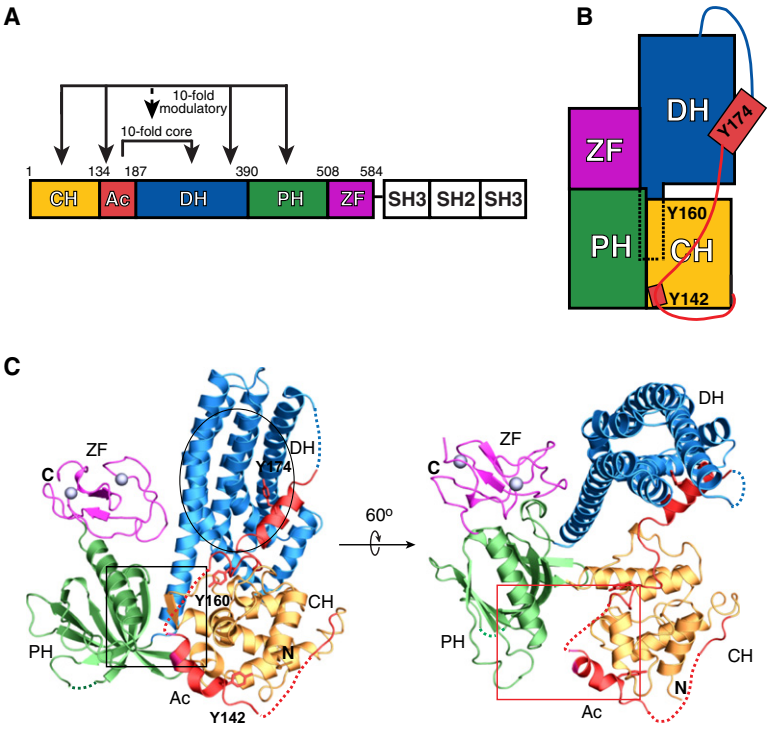

Figure 1. Structural and Energetic Models of Autoinhibition in Vav1

Domains of Vav1 are colored: CH (gold), Ac (red), DH (blue), PH (green), ZF (magenta), SH3 (white), SH2 (white).

(A) Domain architecture of Vav1 and thermodynamic model for cooperative inhibition. Solid lines represent direct physical contacts; dashed line represents thermodynamic coupling between core and modulatory equilibria.

(B) Schematic representation of autoinhibited CADPZ. Dotted lines outline C-terminal helix of DH domain lying behind PH and CH domains.

(C) Ribbon diagram of Vav1 CADPZ. Dashed lines indicate regions not observed in the electron density map. Side chains of tyrosines 142, 160, and 174 are shown as sticks. DH active site is circled. Boxed areas in left and right panels are expanded in Figures 3A and 3B, respectively.

DPZ element overlay from CADPZ and DPZ/Rac complex (2vrw) and selective side-chain interactions are shown in Figure S1. Figure prepared using Pymol (Delano, 2002).

of Vav1 rapidly fluctuates between a "closed" ground state, where the helix is bound to the active site, and an "open" excited state resembling the phosphorylated form, where the helix is dissociated and melted (Li et al., 2008). The closed state is favored by ~10:1, and correspondingly this equilibrium decreases both GEF activity and the rate of Tyr174 phosphorylation by ~10-fold, reflecting accessibility of the active site and the Tyr174 side chain, respectively. Thus, the ratio of the closed and open states determines the magnitude of autoinhibition and rate of activation of the helix-DH core.

A variety of data indicate that interactions of the CH domain further suppress the activity of the DH domain, and that this suppression is critical for Vav1 function in the cell. For example, the original *vav* oncogene encoded a protein lacking part of the CH domain (Katzav et al., 1989). Later studies showed that CH truncation increases the transforming activity of Vav1 and its homolog Vav3, concomitant with increased GEF activity in vitro and in vivo (Bustelo, 2001; Katzav et al., 1991; Llorca et al., 2005). A cryoelectron microscopy reconstruction of full-length Vav3 has suggested that these effects arise from intramolecular binding of the CH domain to the ZF domain, and to a surface of the DH domain adjacent to the Ac-helix interface (Llorca et al., 2005). But this mechanism has not been examined in atomic resolution structural analyses. Moreover, it is not clear how the CH interactions affect the helix-DH core to control GEF activity. Studies of other multidomain systems have shown that the construction of Vav1, with a core autoinhibitory element whose biochemical activity is modulated by other domains, is widespread (DiNitto et al., 2007; Moarefi et al., 1997; Prehoda et al., 2000; Sondermann et al., 2004; Yohe et al., 2008). Thus, understanding how cooperativity is achieved in Vav1 should inform generally on regulation of multidomain proteins.

Although phosphorylation of Tyr174 is clearly important to Vav1 activation, several pieces of data suggest that the process is more complicated than modification of this single site. In addition to Tyr174, Vav1 is also phosphorylated at two additional sites in the N terminus of the acidic element, Tyr142 and Tyr160 upon receptor stimulation (Lopez-Lago et al., 2000; Miletic et al., 2006). Mutation of these sites increases Vav1 signaling activity, suggesting that they may also contribute to autoinhibition in the wild-type protein and that their phosphorylation could play a role in activation. The mechanisms by which Tyr142 and Tyr160 contribute to regulation of Vav1, and more generally the pathway(s) to Vav1 activation, are not understood.

Here we report the structure of the five-domain regulatory element of Vav1, CADPZ. The structure shows that the CH domain and the N terminus of the Acidic element bind to each other and to a platform formed by the PH domain and a C-terminal extension of the DH domain. Nuclear magnetic resonance (NMR), biochemical, and cell biological analyses show that these interactions suppress GEF activity by modulating the core helix-DH equilibrium, shifting it toward the inhibited state by approximately 10-fold, likely by restraining the inhibitory helix to the DH domain. Phosphorylation of Tyr142 and Tyr160 relieves the modulatory interactions, making Tyr174 more accessible to kinases, suggesting a sequential activation mechanism for full-length Vav1. The layered construction of Vav1 provides a means of achieving strong suppression of activity while still maintaining a route to rapid activation, features that are probably general among multidomain systems in biology.

RESULTS

Structure of Autoinhibited Vav1

To understand how interdomain contacts act together to suppress GEF activity, and how phosphorylation drives activation, we determined the crystal structure of the CADPZ element of Vav1 (Table S1 available online; Figures 1B and 1C) using data to a resolution of 2.73 Å. The core module, consisting of the

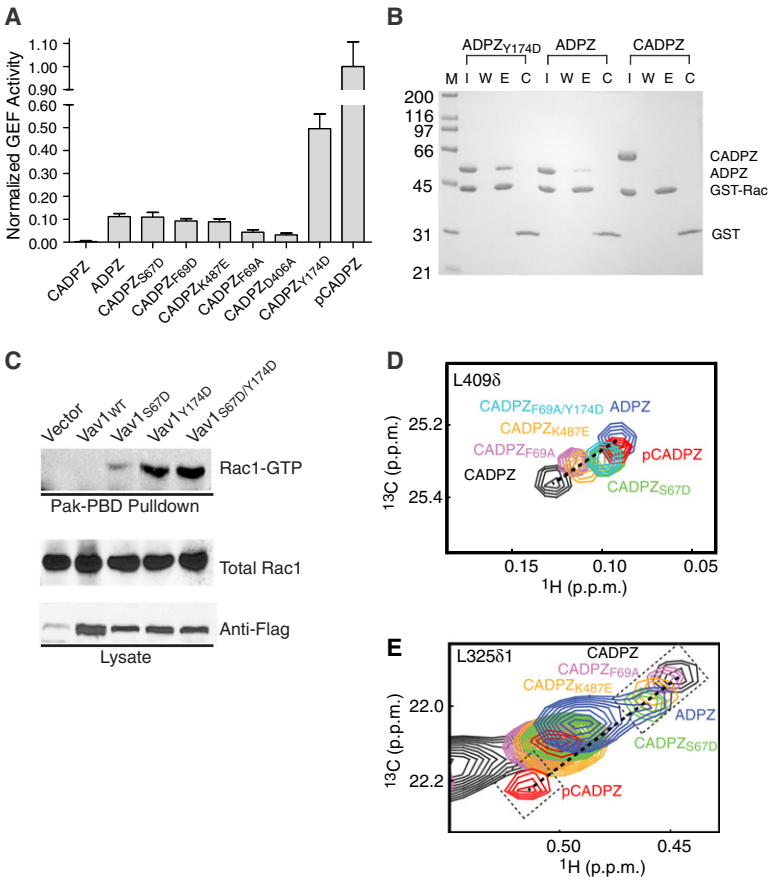

Figure 2. Vav1 Activity Is Cooperatively Suppressed through Energetic Coupling of the Core and Modulatory Equilibria

(A) Normalized GEF activity of human Vav1 proteins. Error bars show standard deviation (SD) from three independent measurements. NMR data showing that phosphorylation causes dissociation of the CH domain are in Figure S2A.

(B) Immobilized GST-Rac(GDP) was used to pull down the indicated Vav1 proteins, which were separated by SDS-PAGE and visualized by Coomassie blue staining. M, I, W, E, C represent molecular-weight markers, input, final wash, elution, and elution from control (GST) beads, respectively.

(C) Panc04.03 cells were transfected with a control vector or the indicated full-length Vav1 expression constructs and analyzed for Rac1(GTP) using GST-Pak-PBD. Proteins were resolved by SDS-PAGE and detected by immunoblotting with the indicated antibodies. Transformation assays of the same Vav1 proteins are in Figures S2B–S2D.

(D) Overlaid $^{1}H/^{13}C$ methyl TROSY spectra of a Leu409δ (CH-PH interface) signal in human CADPZ (black), $CADPZ_{F69A}$ (magenta), $CADPZ_{F69A/Y174D}$ (cyan), $CADPZ_{S67D}$ (green), $CADPZ_{K487E}$ (orange), pCADPZ (red), and ADPZ (blue) proteins.

(E) Overlaid $^{1}H/^{13}C$ methyl TROSY spectra of the Leu325δ1 resonance (DH-helix interface). Spectra colored as in (D).

In (D) and (E), reporter signals are boxed; dashed lines connect endpoints. Spectra showing additional NMR signals are in Figures S2E–S2I.

Tyr174-containing inhibitory helix and DH domain, closely resembles the previously reported solution structure of this fragment (Aghazadeh et al., 2000). The inhibitory helix lies perpendicular to the long axis of the DH domain in the bottom of the active site. The PH and ZF domains dock onto the C terminus and center of an extended C-terminal helix of the DH domain, respectively, and make extensive contacts with each other as well. The organization of the DPZ portion of the structure closely resembles that seen in recently reported structures of the DPZ-Rac complex (Chrencik et al., 2008; Rapley et al., 2008). However, a small bend near the center of the C-terminal DH helix somewhat changes the relative orientations of the DH domain and PZ unit in the two structures (Figures S1A and S1B). The CH domain binds the PH domain and the extended C-terminal helix of the DH domain but does not contact the ZF domain, in contrast to previous inferences from electron microscopy (EM) and biochemical data (Llorca et al., 2005). The CH domain contacts the helix-DH element only through Arg58 (CH), whose side chain is near that of Glu169 (helix).

The Ac element emerges from the side of the CH domain opposite the DH domain. A short N-terminal helix (residues 143–150) wraps around the CH domain and also contacts the PH domain. This is followed by a long extended element (residues 151–166) that connects to the inhibitory helix packed in the DH active site (Figures 1B and 1C). Tyr142 is located immediately before the N-terminal Ac helix; Tyr160 is located in the extended element. Both side chains lie on the surface of the CH domain, with their aromatic rings contacting primarily hydrophobic residues (Tyr142: Val30, Gly106, Ile109, Leu145; Tyr160: Val41, Leu159, Arg63) (Figures S1C and S1D). The hydroxyl group of Tyr160 forms a hydrogen bond with the side chain of Asp39 (Figure S1D).

Validation of the Structure by Mutagenesis

The overall domain organization of the structure here is quite different from the previously reported EM reconstruction of Vav3, which is 58% identical to Vav1 in amino acid sequence (see the Extended Experimental Procedures). Most significantly, the contacts of the CH domain to the PH domain and extended C-terminal helix of the DH domain are not possible in the previous description. To validate the organization observed in the crystal, we mutated a series of residues at different contact surfaces of the CH domain and compared the GEF activity of these proteins to several benchmarks. In the wild-type CADPZ protein, GEF activity is inhibited by the effects of the Acidic helix on the DH active site and by the modulation of this core interaction by the interdomain contacts of the CH domain (referred to as modulatory interactions hereafter). Thus, as shown in Figure 2A, CADPZ has extremely low GEF activity toward Rac. Truncation of the CH domain (giving the ADPZ protein) results in partial activation, consistent with the absence of modulatory interactions of the CH domain but the remaining presence of the core inhibitory

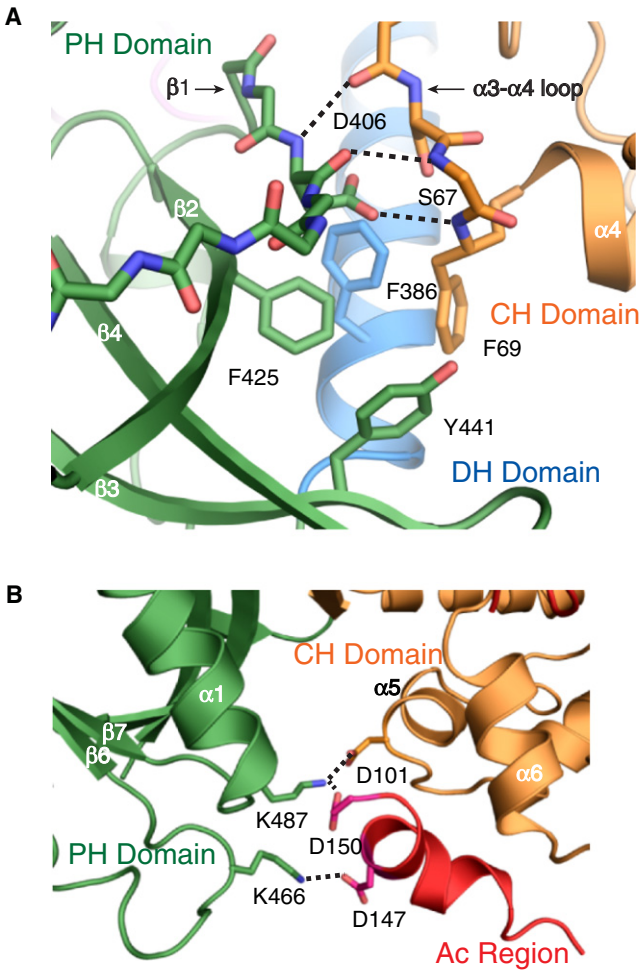

Figure 3. Interdomain Contacts in Vav1

Domains colored as in Figure 1.

(A) Contacts between CH, PH, and DH domains. Residues discussed in the text are shown as sticks.

(B) Contacts between CH domain, Ac region, and PH domain. Potential hydrogen bonds and ionic interactions are shown as dashed lines. Regions shown in (A) and (B) are boxed in black and red, respectively, in Figure 1C.

interaction of the Acidic helix with the DH active site. Phosphorylation of CADPZ at all three tyrosine sites in the Acidic region (giving pCADPZ) disables both the modulatory and core elements of the autoinhibitory apparatus (Figure S2A), leading to maximal GEF activity. GEF activity of fully active (mimicked by $ADPZ_{Y174D}$), partially active (ADPZ), and maximally inhibited (CADPZ) proteins parallels affinity for Rac, as qualitatively assessed in pull-down assays (Figure 2B), further supporting the idea that activity reflects accessibility of the DH active site (Li et al., 2008).

The activities of wild-type CADPZ, ADPZ, and pCADPZ provide reference points for analysis of a series of CADPZ mutants. These were designed based on the structure of the CH-Ac interface with the DPZ element (Figure 3). The CH-Ac element contacts DPZ through two groups of residues. In the first group, the α3-α4 loop of the CH domain (residues 66–68) makes parallel β sheet-like interactions with the first β strand of the PH domain (residues 406–408); interstrand hydrogen bonds are observed between the side chain of Asp406 and the main chain NH of Phe69, and Ser67 is immediately adjacent to Asp406 (Figure 3A). Additional contacts in this region occur within a hydrophobic cluster that contains Phe69 (CH), Phe425 (PH), Tyr441 (PH), and Phe386 (DH extended helix). The second interaction group is immediately adjacent, with the N-terminal helix of the Ac element contacting the basic β5-β6 and β7-α1 loops of the PH domain. Several oppositely charged side chains are in close proximity across this interface, including Asp150 (Ac) and Lys487 (PH) (Figure 3B). CADPZ mutations S67D, F69D, and K487E were designed to strongly destabilize the β strand, hydrophobic cluster, and Ac-PH interactions, respectively. These CADPZ mutants had GEF activity ~10% of pCADPZ, very similar to that of ADPZ, which lacks the CH domain entirely. F69A and D406A mutations caused smaller increases in GEF activity, consistent with less severe perturbations of the CH interactions (Figure 2A). Mutation of Met66, a residue near the CH-PH interface but making no interdomain contacts, had no effect on GEF activity (not shown). Our crystal structure is also consistent with the activities of several previously reported CH domain mutants (Figures S1E–S1G; Table S2).

The GEF activity of Vav1 is also manifest in signaling strength in cells. Previous reports have shown that overexpression of Vav1 proteins lacking the CH domain leads to increased Rac activation and cell transformation (Bustelo, 2001; Han et al., 1998; Llorca et al., 2005; Lopez-Lago et al., 2000), consistent with the increased GEF activity of the ADPZ protein. Further truncation to remove the Ac domain inhibitory helix increases cellular activity further (Abe et al., 1999), consistent with loss of the core inhibitory element. As shown in Figure 2C, destabilizing the modulatory interactions through the S67D mutation also increases Rac activation in cells. Rac activation is higher in cells expressing the Y174D helix mutant, consistent with higher GEF activity of the corresponding CADPZ protein (Figure 2A), and in the S67D/Y174D double mutant. Similar behavior is observed in focus-forming assays, where wild-type Vav1 is much less active than the S67D, Y174D, and double mutants (Figures S2B–S2D). The similarity in this assay between the three mutants likely arises because the long timecourse of the assay flattens differences between partially and fully active proteins. Nevertheless these data suggest that the additional modulatory interactions are relevant for the control of Vav activity under nonstimulated conditions. The combined biochemical and biological data validate the crystal structure and illustrate the importance of the modulatory contacts in controlling GEF activity in vitro and in vivo.

Energetic and Structural Mechanisms of Autoinhibition

The data above demonstrate that the modulatory interactions of the CH and Ac elements with the PH domain further suppress the GEF activity of the helix-DH core. However, they do not reveal how this suppression occurs. One possibility is that interactions of the CH domain shift the autoinhibitory helix-DH equilibrium to further favor the helix-bound state. That is, the helix-DH equilibrium may be thermodynamically coupled to the intramolecular binding equilibria of the CH domain such that the bound state

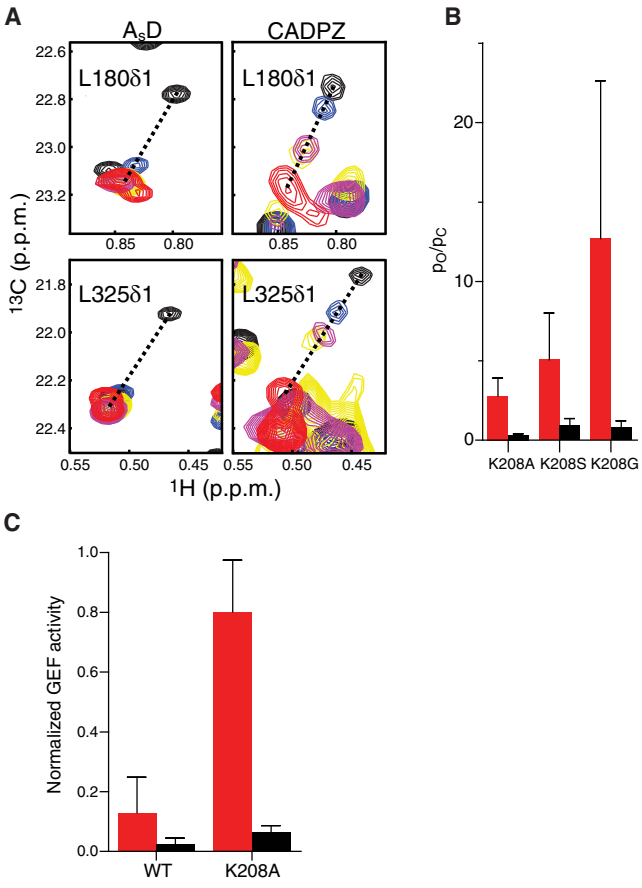

Figure 4. Interdomain Cooperativity in Vav1

(A) Overlaid $^{1}H/^{13}C$ methyl TROSY spectra of murine A_sD and CADPZ proteins (left and right panels, respectively), showing Leu180δ1 and Leu325δ1 signals (top and bottom panels, respectively). Colors are as follows: wild-type (WT) (black), K208A (blue), K208S (yellow), K208G (magenta) mutants and pA_sD or $CADPZ_{Y174D}$ (red). Relaxation dispersion data for A_sD, AD, CAD, CADPZ, and methyl TROSY spectra showing additional NMR signals are in Figures S3. Dotted lines connect resonances from phosphorylated and nonphosphorylated proteins.

(B) Ratio of open and closed populations (p_o/p_c, average ± SD from 5–8 resonances) of murine A_sD (red bars) and CADPZ (black bars) proteins.

(C) Normalized GEF activity of murine A_sD (red; previously shown in Li et al., 2008 and reproduced here by permission from Macmillan Publishers Ltd) and CADPZ proteins (black). Error bars show SD from three independent measurements.

of one favors the bound state of the other and vice versa. Although analogous mechanisms have been proposed to explain interdomain cooperativity in other multidomain systems (DiNitto et al., 2007; Prehoda et al., 2000; Sondermann et al., 2004; Young et al., 2001), these hypotheses have not to our knowledge been tested by direct measurement of the regulatory equilibria.

To test this hypothesis here, we used NMR to directly examine the autoinhibitory helix-DH equilibrium in the A_sD protein (where A_s indicates a shortened Acidic region containing only the inhibitory helix) and CADPZ. We recently showed that in A_sD the inhibitory helix fluctuates in and out of the DH active site on a μs-ms timescale, with the helix-bound and helix-free states in an ~10:1 ratio (Li et al., 2008). These fluctuations are reflected in a large chemical exchange contribution to transverse relaxation of NMR signals arising from methyl groups in the protein (large ΔR_2, the difference between multiple quantum $^{1}H/^{13}C$ transverse relaxation measured at the lowest and highest transverse fields; Figure S3A; Korzhnev et al., 2004). In CADPZ, seven methyl signals that report on the helix-DH interactions are sufficiently free of overlap to be analyzed quantitatively: Leu177δ1 and Leu180δ1,2 from the helix, Val183γ1,2 from the helix-DH linker, and Leu325δ1,2 from the DH domain. ΔR_2 values for all these methyl groups are significantly reduced in CADPZ (Figure S3A), indicating a shift in populations toward the helix-bound state, a change in the fluctuation rate, or both. This reduction in ΔR_2 requires more than addition of the CH domain, as CAD and AD proteins have very similar values (Figure S3A).

We used a chemical shift-based approach to quantify the populations of helix-bound and helix-dissociated states in A_sD and CADPZ. The approach is based on the fact that if a system is fluctuating rapidly (fast exchange) between two states, then the chemical shift of any NMR signal will be a population-weighted average of the chemical shifts of the pure states. Thus, when the chemical shifts of the pure states are known (or can be approximated), the chemical shift observed for any given protein reports on the relative populations of the two states in equilibrium. Using this approach we recently showed that a designed series of A_sD mutants have different populations of helix-bound and helix-dissociated states across the autoinhibitory equilibrium (Li et al., 2008). These proteins ranged from ~5% to >99% open. When their NMR spectra are overlaid, their signals lie on linear trajectories between those of pA_sD and a nearly completely closed mutant. Three of the mutants, K208A, K208S, and K208G, populate predominantly the open state of A_sD, with open populations of 74% ± 10%, 83% ± 9%, and 93% ± 6%, respectively (Li et al., 2008). To determine if the helix-DH equilibrium is different in CADPZ, here we examined methyl TROSY spectra of CADPZ proteins containing these same three mutations, as well as a Y174D mutant of CADPZ ($CADPZ_{Y174D}$) that mimics the phosphorylated protein (not shown). As shown in Figure 4A, methyl chemical shifts from the helix and DH elements in pA_sD and $CADPZ_{Y174D}$ are nearly identical, indicating that phosphorylation also shifts the helix-DH equilibrium in CADPZ to strongly favor the helix-dissociated state (Figure 4A; Figures S3B–S3D). Similarly, the helix and DH chemical shifts are in similar positions in A_sD and CADPZ. Thus, the open and closed forms of the helix-DH element are very similar in A_sD and CADPZ. Five of the interface methyl resonances in the CADPZ mutants are in fast exchange and free of overlap. As in A_sD (Li et al., 2008), these resonances lie along the linear trajectory between the nonphosphorylated and phosphorylated chemical shifts (Figure 4A; Figures S3B–S3D). This linearity indicates that from the standpoint of the inhibitory interface, CADPZ exists in an equilibrium analogous to that in A_sD, fluctuating between helix-bound and helix-dissociated states. However, for each mutant, the signals in CADPZ are shifted appreciably toward the nonphosphorylated position relative to those in A_sD. Thus, the core inhibitory equilibrium is shifted toward the helix-bound state in CADPZ (Figure 4A). These data

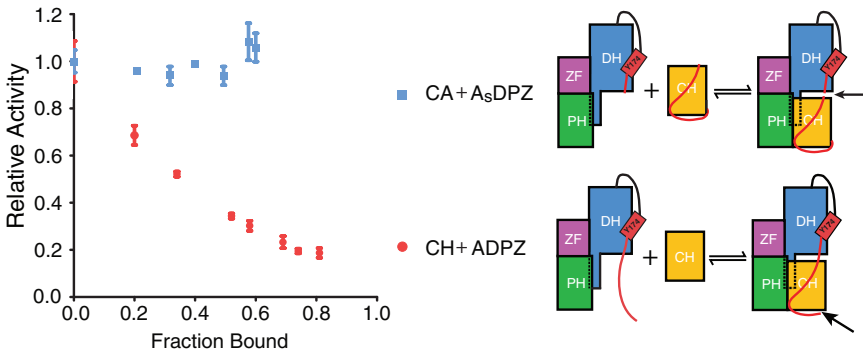

Figure 5. Inhibitory Effects of the CH Domain Require an Intact Ac Element

Relative GEF activity in titrations of CH proteins into ADPZ proteins: CH+ADPZ (red circles), CA+A_sDPZ (blue squares). Activities were normalized to those of free ADPZ or A_sDPZ. Error bars represent SD from three independent measurements. Cartoon on the right depicts the corresponding titration reaction. Arrow indicates the position where the Ac element is cut. NMR titrations and comparison of CH titration into ADPZ with control experiments are shown in Figures S4.

are consistent with the reduction of ΔR_2 in wild-type CADPZ observed above. The observed chemical shifts indicate that on average the equilibrium is shifted ~10-fold for each mutant (range = 6- to 16-fold) (Figure 4B). The shift in equilibrium toward the helix-bound state is also manifest in GEF activity. As in the A_sD proteins (Li et al., 2008), GEF activity of CADPZ is appreciably lower than that of $CADPZ_{K208A}$, reflecting destabilization of autoinhibitory contacts in the mutant (black bars in Figure 4C). Most importantly, the activities of the CADPZ proteins are significantly below those of their A_sD counterparts due to the decreased accessibility of the DH active site (compare black and red bars in Figure 4C).

These NMR data indicate a thermodynamic mechanism of interdomain cooperativity in which the 10-fold suppression of accessibility of the DH active site caused by the intrinsic thermodynamics of the A_sD core is enhanced an additional 10-fold by modulatory interactions of the CH domain. How is coupling between these equilibria achieved structurally? In this regard, the paucity of contacts between the CH domain and the helix-DH core element is striking (Figure 1C, right panel). Mutation of the lone direct CH-DH contact observed in the crystal (R58A) has no effect on GEF activity in CADPZ (not shown). This suggests that the CH domain acts on GEF activity in an indirect manner, perhaps by restraining the N terminus of the Acidic domain against the DPZ element and consequently entropically disfavoring the dissociated state of the inhibitory helix. One prediction of this structural mechanism is that cutting the Acidic element immediately before the helix should destroy the mechanical linkage between the modulatory and core elements, preventing the CH domain from affecting GEF activity. To test this hypothesis, we performed two titrations, monitoring GEF activity (Figure 5). In the first, we added CH (residues 1–134) to ADPZ (residues 135–584), an interaction with a dissociation equilibrium constant (K_D) of 32 μM based on independent NMR analyses (not shown). As illustrated in Figure 5, the CH domain can act in *trans* to suppress GEF activity of ADPZ, with activity decreasing linearly with the fraction bound. Thus, a protein cleaved at the CH-Acidic junction can manifest coupling between the modulatory and core equilibria (see also Figures S4A–S4C). This effect is specific, as titrations of CH_{S67D} into ADPZ or CH into $ADPZ_{K487E}$ produced much less inhibition (Figure S4D). In contrast, addition of a CA construct lacking the inhibitory helix (residues 1–168) to A_sDPZ (residues 169–584, K_D = 290 μM) had no effect on GEF activity. Thus, cleaving the Ac element before the inhibitory helix prevents the modulatory equilibrium from communicating to the core equilibrium. In an analogous titration of CA into deuterated, methyl protonated A_sDPZ, monitored by methyl TROSY spectra of A_sDPZ, resonances at the CH-PH interface moved linearly from their positions in free A_sDPZ toward their positions in CADPZ (Figures S4E and S4F). Thus, the complex reproduced many of the packing interactions of the intact protein. In the same titration, resonances at the helix-DH interface were not affected, indicating that the helix-DH equilibrium is not affected by CH-PH interactions when the Ac element is broken (Figure S4G, compare to Figure S4C). Thus, the decrease in GEF activity tracks with modulation of the helix-DH equilibrium, not simply binding of the CH domain to the PH domain. The data are consistent with the idea that the modulatory interactions act on the helix-DH equilibrium by restraining the N terminus of the Ac element, disfavoring dissociation of the helix.

Validation of the Energetic Mechanism by Mutagenesis

To investigate the idea of coupled equilibria in greater detail, we examined the NMR properties of the proteins described above (Figure 2A), which are impaired in one or both elements of the inhibitory apparatus (modulatory or core inhibitory interactions). For each protein we examined two sets of NMR signals. The first consists of methyl groups located at the CH-PH interface (Leu409δ1,2, Leu491δ, Val102γ; Figures 2D; Figures S2E–S2G). If the CH domain equilibrates rapidly between the state observed in the crystal structure (with contacts to Ac and PH intact) and a state where the contacts to Ac and PH are lost, then the chemical shifts of these methyl signals should reflect the populations of the two states. This is exactly analogous to our analysis of the helix-DH equilibrium in Figure 4, under the assumption that contacts of the CH domain to Ac and PH are highly cooperative (i.e., CH is either fully bound to both elements or fully dissociated). When interactions between the CH and PH domains in CADPZ are destabilized by mutation, these "CH-PH signals," which report on stability of the modulatory interactions, will shift toward the dissociated extreme. The bound extreme is represented by the CADPZ chemical shifts, and the dissociated extreme by the chemical shifts of ADPZ or pCADPZ, where the modulatory contacts are absent or fully destabilized, respectively (Figure 2D; Figure S2A). For each protein we also examined NMR signals of methyl groups at the helix-DH interface (Figure 2E; Figures S2H and S2I). As in Figure 4, these signals

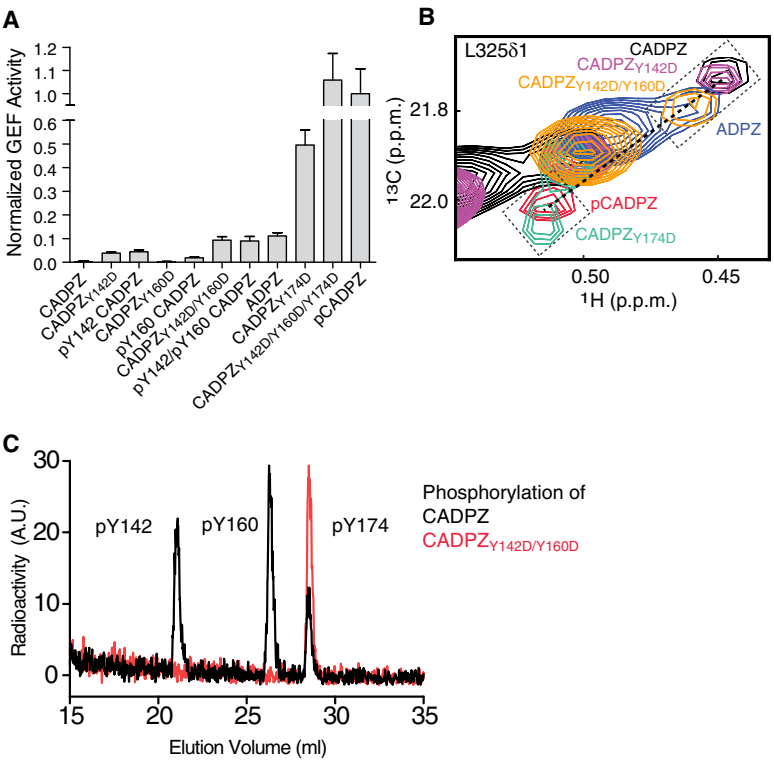

Figure 6. Initial Phosphorylation of Tyr142 and Tyr160 Can Provide a Route to Full Vav1 Activation

(A) Normalized GEF activity of human Vav1 proteins. Error bars represent SD from three independent measurements.

(B) Overlaid $^{1}H/^{13}C$ methyl TROSY spectra of the Leu325δ1 signal (boxed) in human CADPZ (black), ADPZ (blue), and $CADPZ_{Y142D}$ (magenta), $CADPZ_{Y174D}$ (green), $CADPZ_{Y142D/Y160D}$ (gold), pCADPZ (red) proteins. Spectra showing additional NMR signals and relaxation dispersion analysis of CADPZ are in Figures S5.

(C) HPLC analysis (with scintillation detection) of tryptic digests of CADPZ (black) and $CADPZ_{Y142D/Y160D}$ (red) after phosphorylation with [γ-^{32}P] ATP for 7.5 min. Peaks corresponding to pTyr142-, pTyr160-, and pTyr174-containing peptides are indicated. At complete phosphorylation, the peak corresponding to pY174 has virtually identical amplitude for the two proteins (not shown). HPLC analysis of tryptic digests of CADPZ and $CADPZ_{D39N}$ after phosphorylation with [γ-^{32}P] ATP are in Figures S5.

report on populations across the core inhibitory equilibrium. By comparing CH-PH and helix-DH signals for each mutant, we can observe how changes to one process affect the other. We can also correlate both to GEF activity. The behavior of ADPZ is demonstrative. In this protein the CH-PH signals are strongly shifted from their CADPZ positions, reflecting the absence of modulatory interactions. In contrast, since the core inhibitory module is intact, the helix-DH signals in ADPZ are shifted only partially from the CADPZ positions toward the pCADPZ positions (Figure 2E). The GEF activity of ADPZ, which is dependent on exposure of the DH active site, parallels the helix-DH signals (Figure 2A). In the CADPZ mutants S67D, F69D, and K487E, which were designed to destabilize the modulatory interactions, the CH-PH signals shift appreciably toward their open positions (Figure 2D). The helix-DH signals shift toward the open position but remain in the range between the CADPZ and ADPZ positions (Figure 2E). These changes are consistent with the GEF activities of these mutants, which are at or below that of ADPZ (Figure 2A). The less perturbing mutations F69A and D406A show smaller shifts in the CH-PH signals, much smaller shifts in the helix-DH signals (Figure 2E), and lower GEF activity (Figure 2A). Thus, shifting the modulatory equilibrium changes the helix-DH equilibrium and consequently GEF activity. Perturbations can also be observed in reciprocal fashion: introducing the Y174D (helix) mutation into the F69A background shifts the CH-PH signals toward their positions in ADPZ (Figure 2D). Thus, destabilizing the helix-DH interactions also destabilizes the modulatory interactions. These data support our model that the core and modulatory equilibria are thermodynamically coupled, and that this coupling is a major contributor to the cooperative suppression of GEF activity by interactions of the CH domain.

Vav1 Activation by Multisite Phosphorylation

Our model for autoinhibition creates a conundrum regarding activation of Vav1. That is, how is Tyr174 rapidly accessed by kinases, as is known to occur in vivo (Miletic et al., 2006), when its exposure is strongly suppressed by the combined actions of the core and modulatory equilibria? We asked whether the Tyr142 and Tyr160 phosphorylation sites could be important in providing a kinetic pathway to activation. As shown in Figure 6A, phosphorylation at Tyr160 or Tyr142 had little effect on GEF activity. However, the doubly phosphorylated pTyr142/pTyr160 protein has activity similar to ADPZ. To generate materials on larger scale we mimicked phosphorylation by mutation of Tyr142 and/or Tyr160 to aspartate. The Tyr to Asp mutants have GEF activity very similar to their pTyr counterparts, indicating that the mutations act similarly to phosphorylation. The change in activity of the mutants occurs concomitantly with a shift in the helix-DH equilibrium toward the ADPZ position as assessed by NMR (Figure 6B; Figures S5A and S5B). A Y142F/Y160F double mutant has GEF activity and NMR properties similar to the double Asp mutant (not shown), explaining previous data showing that Y142F and Y160F mutations increase the transforming activity of Vav1 (Lopez-Lago et al., 2000). These data suggest that initial phosphorylation at Tyr142 and Tyr160 could destabilize the modulatory interactions, increasing access of Tyr174 to kinases. In support of this model, Tyr174 is phosphorylated by the Lck kinase domain much more rapidly in the Y142D/Y160D mutant than in wild-type CADPZ (Figure 6C). Moreover, in wild-type CADPZ, Tyr142 and Tyr160 are phosphorylated more rapidly than Tyr174 (Figure 6C). This is striking because in short peptides containing the different Vav1 tyrosine motifs, phosphorylation of Tyr174 is strongly favored over Tyr142 and Tyr160 (Amarasinghe and Rosen, 2005). These data suggest an ordered pathway dictated by the structural organization of CADPZ in which Tyr142 and Tyr160 are modified initially, followed by Tyr174. Interestingly, mutation of the highly conserved Asp39,

which coordinates the Tyr160 hydroxyl group, to asparagine decreases both the initial rate of phosphorylation of Tyr160 and also the rate of subsequent phosphorylation of Tyr142 and Tyr174 (Figure S5C). Thus, Asp39 may be selected to tune the system into an appropriate response regime.

Tyr142 and Tyr160 would not be accessible to kinases in the conformation observed in the crystal. However, both side chains are on the surface of the protein, and NMR relaxation data indicate substantial μs-ms timescale fluctuations of methyl groups surrounding them in the Ac element (Figure S5D). These dynamics likely represent transitions to kinase-accessible conformations, explaining how Tyr142 and Tyr160 can be phosphorylated rapidly. We previously showed that pTyr142 in Ac peptides provides a docking site for the SH2 domain of the Lck kinase, and that this interaction allows Lck to phosphorylate Tyr174 in unimolecular fashion with increased efficiency (4-fold higher second order catalytic rate constant [k_{cat}/K_M]) (Amarasinghe and Rosen, 2005). Upon initial phosphorylation of Tyr142/Tyr160, destabilization of modulatory contacts and recruitment of kinase should act synergistically to increase phosphorylation of Tyr174 by Lck. Thus, the structural and energetic architecture of Vav1 provides a facile kinetic route to activation in the face of substantial suppression of basal activity. Since Tyr142 and Tyr160 are conserved in 31 of 33 available Vav sequences (*Aedes aegypti* and *Tribolium castaneum* sequences have only Tyr142), this mechanism is likely to be general across the family.

DISCUSSION

Our collective data show that the regulatory apparatus of Vav1 is composed of at least two thermodynamically coupled processes (Figure 1A). A core process, in which the inhibitory helix blocks the DH active site, provides approximately 10-fold suppression of activity and phosphorylation rate (Li et al., 2008). Binding of the CH domain to the N terminus of the Acidic element and to the DPZ fragment restricts the inhibitory helix, thermodynamically coupling these interactions to the core. This coupling shifts the helix-DH equilibrium ~10-fold further toward the inhibited (helix-bound) state. Together, the two processes provide the high level of suppression (~100-fold) that is apparently needed for in vivo function (as CH truncation leads to cell transformation; Bustelo, 2001; Katzav et al., 1991; Llorca et al., 2005). This 10-fold × 10-fold construction of Vav1 (rather than a single 100-fold inhibitory equilibrium) is likely functionally important, as we have shown that inhibition by the core alone can be increased to 50-fold simply by two point mutations (Li et al., 2008). Biochemical data on other multidomain systems suggest similar (relatively small, 2- to 20-fold) magnitudes of core suppression and modulatory coupling (DiNitto et al., 2007; Moarefi et al., 1997).

This construction has important implications for the biology of Vav1. It provides a quantitative rationale for the increased activity of CH domain truncations of the protein. In such truncations, even though the core inhibitory module is intact, the inherent thermodynamics of the module produce high levels of the active state (9%–33%; Figures 2E and 4A; Figure S3A) when coupling to the modulatory equilibrium is lost. This effect increases both the phosphorylation rate (and likely steady-state phosphorylation level) and basal GEF activity of Vav1, explaining increased Rac activation and cell transformation (Bustelo, 2001; Han et al., 1998; Llorca et al., 2005; Lopez-Lago et al., 2000). The ability of CH interactions to modulate the AD core also implies that molecules that disrupt these contacts could partially stimulate Vav1 activity and act cooperatively with kinases to fully activate the protein in vivo.

The creation of suppression from multiple weak interactions also has important implications regarding the kinetics of Vav1 activation upon receptor stimulation. In many allosteric systems, it has been shown that activators gain access to their targets by recognizing the small population of active state present under basal conditions (Henzler-Wildman and Kern, 2007). This is the case in the A_sD core of Vav1, where kinases can only recognize Tyr174 in the helix-dissociated state (Li et al., 2008). However, strong suppression of activity opposes this pathway, as it requires that the accessible population be very small, which would tend to make activation slow. The layered energetic and physical construction of modular proteins provides a likely general solution to this problem, which we have observed for Vav1. That is, the structure and energetics of multidomain systems can be organized so that the modulatory elements are more accessible to activators (e.g., Tyr142 and Tyr160 in the CA element show significant μs-ms timescale dynamics and can be rapidly phosphorylated). This allows activation to occur in stepwise fashion, with initial events disabling the modulatory interactions and consequently increasing access to the core. Thus, modularity enables evolution not only of strong inhibition but also of ready routes to activation.

A variety of biochemical and structural data suggest that the energetic and kinetic mechanisms that we have found for Vav1 are likely to be widespread among multidomain proteins. The Tim family of GEFs represents a structurally and functionally similar example (Yohe et al., 2008). The Tim proteins have a DH domain whose activity is inhibited by an adjacent helix that binds in the active site and that can be displaced by phosphorylation, analogous to the Vav AD core. The Tim proteins also have a C-terminal SH3 domain that further suppresses the activity of the helix-DH core through binding an internal proline-rich motif (PRM). The mechanism of suppression by the SH3 domain has not been explored, but available data would be consistent with coupling of the helix-DH and SH3-PRM equilibria. Moreover, although the kinetic pathway to Tim activation has not been examined experimentally, it has been speculated that activation may occur stepwise, with initial displacement of SH3-PRM interactions facilitating phosphorylation of the inhibitory helix (Yohe et al., 2008). The unrelated Ras GEF, SOS, also appears to use the same regulatory logic, with the DH-PH element shifting an allosteric equilibrium in the Rem-Cdc25 element toward its inactive state (Sondermann et al., 2004).

The broadest class of, and best characterized, proteins that appear to behave in this manner are the protein kinases. A large body of data suggests that the isolated kinase domain fluctuates between an inactive state, where the active site is not properly organized for catalysis, and an active state, where the catalytic cluster and substrate-binding site are catalytically competent (e.g., Levinson et al., 2006; Masterson et al., 2008; Vogtherr

et al., 2006). Phosphorylation of residues in the so-called activation loop stabilizes the active conformation, increasing catalytic activity. Whereas the active state is common among many kinases, the inactive states differ. Sampling of the inactive conformation has been capitalized upon in the Abl tyrosine kinase inhibitor imatinib, a widely used anticancer therapeutic (Schindler et al., 2000). Imatinib distinguishes Abl from other closely related kinases by selectively binding to its unique inactive conformation. NMR analysis of fluctuations between the active and inactive states in isolated kinase domains is an active area of research. However, to date such studies have not yielded a quantitative understanding of kinase thermodynamics (populations of the states) or a detailed view of the equilibrating structures in the absence of stabilizing inhibitors (Masterson et al., 2008; Vajpai et al., 2008; Vogtherr et al., 2006). Many kinases also contain additional domains that repress the activity of the catalytic domain (Huse and Kuriyan, 2002). Disabling such domains, either by truncation or through regulatory interactions, increases the activity of kinases toward various substrates. A detailed interpretation of the biochemical data in terms of allosteric equilibria is complicated by the fact that phosphorylation of the activation loop locks the kinase in an active state, and the activity of nonphosphorylated kinases is very low and thus hard to quantify. However, molecular dynamics simulations of the Src kinase have suggested that, at least in that system, the additional SH3 and SH2 domains suppress activity through biasing the regulatory equilibrium in the kinase domain toward the inactive state (Faraldo-Gomez and Roux, 2007; Young et al., 2001). As in Vav, this construction also appears to dictate that kinases are activated in stepwise fashion, with initial events that disable modulatory interactions (e.g., in Src by ligand binding to the SH3 domain; Moarefi et al., 1997) enabling phosphorylation of the activation loop and consequent maximum stabilization of the active state.

These various examples strongly suggest that although multidomain proteins use a variety of structural mechanisms to achieve regulation, the underlying energetic mechanism that we have illustrated for Vav, and the requirement for an ordered activation process that arises from it, are likely to be widely observed. The NMR approach we developed here provides a means to directly measure the populations of different states across regulatory equilibria and has allowed us to quantitatively characterize the energetic landscape of Vav1. This in turn has established coupled equilibria as a major mechanism of interdomain cooperativity in this system. Application of these methods to other systems should reveal how widespread cooperative inhibition through coupled equilibria is in multidomain proteins.

EXPERIMENTAL PROCEDURES

Generation of Materials

Detailed expression, modification, and purification procedures for all materials are provided in the Extended Experimental Procedures.

Quantitative Phosphorylation of Tyr142, Tyr160, and Tyr174

We created a murine CADPZ mutant ($CADPZ_{tryp}$) containing three additional tryptic sites: Arg135, Lys148, and Lys166. Trypsinolysis of $CADPZ_{tryp}$ yields peptides containing Tyr142 (136–148), Tyr160 (149–166), and Tyr174 (167–179). Most NMR signals that report on the core and modulatory equilibria are in identical positions in CADPZ and $CADPZ_{tryp}$ (not shown), suggesting that phosphorylation of $CADPZ_{tryp}$ is representative of wild-type. Moreover, bulk phosphorylation kinetics of CADPZ and $CADPZ_{tryp}$ are identical (not shown). Lck-mediated phosphorylation reactions were carried out with [γ^{32}P]ATP, quenched with the kinase inhibitor LckI2 (Calbiochem #428206), and urea to 8M. Proteins were digested with trypsin. Peptides containing pTyr142, pTyr160, and pTyr174 were separated with reverse-phase HPLC and detected by an in-line scintillation counter (Bioscan Flow-Count). See Extended Experimental Procedures for details.

Crystallization and X-Ray Diffraction Data Collection

Crystals of human Vav1 CADPZ (~50 × 100 × 200 μm) were grown at 4°C using the hanging-drop vapor-diffusion method. Drops contained 2 μl of 3–10 mg/ml protein solution (20 mM Tris [pH 7.5], 50 mM NaCl, 5% [w/v] glycerol, 2 mM TCEP) and were equilibrated against 200 μl of water. Crystals of selenomethionine-labeled protein were obtained under similar conditions when seeded with native crystals. Crystals were cryoprotected by addition of ethylene glycol to 30% (v/v). Native and anomalous dispersion data were collected at 100 K using the Advanced Photon Source 19ID beamline. The native dataset was collected at the anomalous edge for zinc. Vav1 CADPZ crystallized in space group $P2_1$ with unit cell parameters of a = 85 Å, b = 59 Å, c = 161 Å, β = 97°, containing two molecules in the asymmetric unit with ~55% solvent. Crystals diffracted X-rays to a minimum Bragg spacing of ~2.65 Å. Data were processed using the HKL3000 suite of programs (Minor et al., 2006). Data collection statistics are in Table S1.

Phase Determination and Structure Refinement

Phases were obtained from a single-wavelength anomalous dispersion experiment using a seleno-methionine-Vav1 CADPZ crystal with data to a resolution of 2.80 Å. Thirty of thirty-four expected selenium sites were located using the program SHELXD (Schneider and Sheldrick, 2002). Phases were refined with the program MLPHARE (Otwinowski, 1991), resulting in a figure-of-merit of 0.27. Phases were further improved by density modification and two-fold noncrystallographic averaging with the program DM (CCP4, 1994) resulting in a figure-of-merit of 0.88. An initial model containing about 54% of all residues was automatically generated using the program ARP/warp (Morris et al., 2004). Additional residues were manually added using the program coot (Emsley and Cowtan, 2004). Refinement was carried out with native data to a resolution of 2.73 Å in the program PHENIX (Adams et al., 2002) and consisted of simulated annealing, conjugate-gradient minimization, and refinement of individual B-factors and TLS parameters, interspersed with manual revisions of the model. The current model contains two Vav1 CADPZ monomers (labeled A and B, respectively) in the asymmetric unit with backbone root-mean-square deviation (rmsd) of 0.13 Å for residues 2–129, 142–150, 156–180, 189–417, 419–456, 463–478, 482–564. Statistics of refinement and structural quality are listed in Table S1.

NMR Spectroscopy

NMR analyses were performed in buffer containing 20 mM Tris(hydroxymethyl-d_3)amino-d_2-methane, pH 7.5 (uncorrected), 100 mM NaCl, 2 mM TCEP, and 10% (w/v) d_8-glycerol; 99.9% D_2O. Data were acquired on 600 and 800 MHz Varian Inova spectrometers equipped with cold probes. CPMG experiments were performed using a constant relaxation period of 20 ms at 15°C. Methyl-TROSY experiments were performed at 25°C. Average open populations (p_o) for murine proteins were determined as previously described (Li et al., 2008). Note that p_o values for A_sD reported here differ slightly from those reported previously due to small differences in buffer conditions. NMR reporters in CADPZ and ADPZ were assigned to residue number by mutagenesis and confirmed by comparison to spectra of A_sD and CAD. Methyl groups at the helix-DH interface of CADPZ/ADPZ were stereospecifically assigned by comparison to signals in A_sD (Aghazadeh et al., 2000).

Guanine Nucleotide Exchange Assays

Guanine nucleotide exchange assays were carried out and analyzed as previously described (Li et al., 2008). Assays contained 10 μM Vav1 CADPZ, A_sDPZ, or ADPZ. In titrations of Figure 5, binding affinities used to calculate fraction bound (see text) were determined independently under identical solution

conditions through NMR titrations of unlabeled ADPZ proteins into methyl-labeled CH-containing proteins.

GST-Rac Pull-Down Assays

In each assay, 10 μM GST-Rac (GDP), 10 μM Vav protein, 0.5 μM GDP, 2 mM $MgCl_2$, and 0.1 M Tris (pH 7.5) were premixed to final volume of 200 μl and bound to 100 μl glutathione sepharose beads (GE Healthcare). After three washes, proteins were eluted with 30 mM glutathione. In control experiments, 10 μM GST was used instead of GST-Rac.

Cell-Based Assays

To measure Rac activation by various full-length Vav1 proteins, Panc04.03 pancreatic cancer cells were transfected with 20 μg of pCDNA3 control vector or Vav1 expression vectors. The GTP-bound form of endogenous Rac1 was detected using the standard GST-PAK affinity precipitation assay 18 hr post-transfection (see Extended Experimental Procedures). The transformation of NIH 3T3 cells was assayed 14 days after transfection with control or Vav1-expressing pCDNA3.1/HisA vector by staining cells with 0.4% crystal violet and counting foci (see Extended Experimental Procedures).

ACCESSION NUMBERS

The coordinates and structure factors have been deposited in the Protein Data Bank under accession number 3KY9.

SUPPLEMENTAL INFORMATION

Supplemental Information includes Extended Experimental Procedures, five figures, and two tables and can be found with this article online at doi:10.1016/j.cell.2009.12.033.

ACKNOWLEDGMENTS

We thank Carlos Amezcua and Chad Brautigam for technical assistance, Lewis Kay for providing NMR pulse sequences, Shae Padrick and Rama Ranganathan for discussion, and Yuh Min Chook for critical reading of the manuscript. I.R.S.M. was supported by fellowships from the Foundation for Science and Technology (Portugal) and the Luso-American Development Foundation (Portugal). G.K.A. was supported by a postdoctoral fellowship from the Cancer Research Institute. This work was supported by NIH grants GM066930 to M.K.R., AI065474 and CA102721 to D.D.B., and CA102721 and CA136526 to M.E.F. and by the Howard Hughes Medical Institute. D.D.B. is a Leukemia and Lymphoma Society Scholar. Use of the Argonne National Laboratory Structural Biology Center beamlines at the Advanced Photon Source was supported by the U.S. Department of Energy, Office of Energy Research, under Contract No. W-31-109-ENG-38.

Received: May 26, 2009
Revised: October 9, 2009
Accepted: December 17, 2009
Published: January 21, 2010

REFERENCES

Abe, K., Whitehead, I.P., O'Bryan, J.P., and Der, C.J. (1999). Involvement of NH(2)-terminal sequences in the negative regulation of Vav signaling and transforming activity. J. Biol. Chem. *274*, 30410–30418.

Adams, P.D., Grosse-Kunstleve, R.W., Hung, L.W., Ioerger, T.R., McCoy, A.J., Moriarty, N.W., Read, R.J., Sacchettini, J.C., Sauter, N.K., and Terwilliger, T.C. (2002). PHENIX: building new software for automated crystallographic structure determination. Acta Crystallogr. D Biol. Crystallogr. *58*, 1948–1954.

Aghazadeh, B., Lowry, W.E., Huang, X.Y., and Rosen, M.K. (2000). Structural basis for relief of autoinhibition of the Dbl homology domain of proto-oncogene Vav by tyrosine phosphorylation. Cell *102*, 625–633.

Amarasinghe, G.K., and Rosen, M.K. (2005). Acidic region tyrosines provide access points for allosteric activation of the autoinhibited Vav1 Dbl homology domain. Biochemistry *44*, 15257–15268.

Bustelo, X.R. (2001). Vav proteins, adaptors and cell signaling. Oncogene *20*, 6372–6381.

Chrencik, J.E., Brooun, A., Zhang, H., Mathews, I.I., Hura, G.L., Foster, S.A., Perry, J.J., Streiff, M., Ramage, P., Widmer, H., et al. (2008). Structural basis of guanine nucleotide exchange mediated by the T-cell essential Vav1. J. Mol. Biol. *380*, 828–843.

CCP4 (Collaborative Computational Project, Number 4). (1994). The CCP4 suite: programs for protein crystallography. Acta Crystallogr. D Biol. Crystallogr. *50*, 760–763.

Cowan, C.W., Shao, Y.R., Sahin, M., Shamah, S.M., Lin, M.Z., Greer, P.L., Gao, S., Griffith, E.C., Brugge, J.S., and Greenberg, M.E. (2005). Vav family GEFs link activated Ephs to endocytosis and axon guidance. Neuron *46*, 205–217.

Delano, W.L. (2002). The PyMOL Molecular Graphics System DeLano Scientific (CA, USA: San Carlos).

DiNitto, J.P., Delprato, A., Gabe Lee, M.T., Cronin, T.C., Huang, S., Guilherme, A., Czech, M.P., and Lambright, D.G. (2007). Structural basis and mechanism of autoregulation in 3-phosphoinositide-dependent Grp1 family Arf GTPase exchange factors. Mol. Cell *28*, 569–583.

Dong, Z., Liu, Y., Lu, S., Wang, A., Lee, K., Wang, L.H., Revelo, M., and Lu, S. (2006). Vav3 oncogene is overexpressed and regulates cell growth and androgen receptor activity in human prostate cancer. Mol. Endocrinol. *20*, 2315–2325.

Emsley, P., and Cowtan, K. (2004). Coot: model-building tools for molecular graphics. Acta Crystallogr. D Biol. Crystallogr. *60*, 2126–2132.

Faraldo-Gomez, J.D., and Roux, B. (2007). On the importance of a funneled energy landscape for the assembly and regulation of multidomain Src tyrosine kinases. Proc. Natl. Acad. Sci. USA *104*, 13643–13648.

Hall, A.B., Gakidis, M.A., Glogauer, M., Wilsbacher, J.L., Gao, S., Swat, W., and Brugge, J.S. (2006). Requirements for Vav guanine nucleotide exchange factors and Rho GTPases in FcgammaR- and complement-mediated phagocytosis. Immunity *24*, 305–316.

Han, J., Luby-Phelps, K., Das, B., Shu, X., Xia, Y., Mosteller, R.D., Krishna, U.M., Falck, J.R., White, M.A., and Broek, D. (1998). Role of substrates and products of PI 3-kinase in regulating activation of Rac-related guanosine triphosphatases by Vav. Science *279*, 558–560.

Henzler-Wildman, K., and Kern, D. (2007). Dynamic personalities of proteins. Nature *450*, 964–972.

Huse, M., and Kuriyan, J. (2002). The conformational plasticity of protein kinases. Cell *109*, 275–282.

Katzav, S. (2007). Flesh and blood: the story of Vav1, a gene that signals in hematopoietic cells but can be transforming in human malignancies. Cancer Lett. *255*, 241–254.

Katzav, S., Cleveland, J.L., Heslop, H.E., and Pulido, D. (1991). Loss of the amino-terminal helix-loop-helix domain of the vav proto-oncogene activates its transforming potential. Mol. Cell. Biol. *11*, 1912–1920.

Katzav, S., Martin-Zanca, D., and Barbacid, M. (1989). vav, a novel human oncogene derived from a locus ubiquitously expressed in hematopoietic cells. EMBO J. *8*, 2283–2290.

Korzhnev, D.M., Kloiber, K., Kanelis, V., Tugarinov, V., and Kay, L.E. (2004). Probing slow dynamics in high molecular weight proteins by methyl-TROSY NMR spectroscopy: application to a 723-residue enzyme. J. Am. Chem. Soc. *126*, 3964–3973.

Levinson, N.M., Kuchment, O., Shen, K., Young, M.A., Koldobskiy, M., Karplus, M., Cole, P.A., and Kuriyan, J. (2006). A Src-like inactive conformation in the abl tyrosine kinase domain. PLoS Biol. *4*, e144.

Li, P., Martins, I.R., Amarasinghe, G.K., and Rosen, M.K. (2008). Internal dynamics control activation and activity of the autoinhibited Vav DH domain. Nat. Struct. Mol. Biol. *15*, 613–618.

Llorca, O., Arias-Palomo, E., Zugaza, J.L., and Bustelo, X.R. (2005). Global conformational rearrangements during the activation of the GDP/GTP exchange factor Vav3. EMBO J. *24*, 1330–1340.

Lopez-Lago, M., Lee, H., Cruz, C., Movilla, N., and Bustelo, X.R. (2000). Tyrosine phosphorylation mediates both activation and downmodulation of the biological activity of Vav. Mol. Cell. Biol. *20*, 1678–1691.

Masterson, L.R., Mascioni, A., Traaseth, N.J., Taylor, S.S., and Veglia, G. (2008). Allosteric cooperativity in protein kinase A. Proc. Natl. Acad. Sci. USA *105*, 506–511.

Miletic, A.V., Sakata-Sogawa, K., Hiroshima, M., Hamann, M.J., Gomez, T.S., Ota, N., Kloeppel, T., Kanagawa, O., Tokunaga, M., Billadeau, D.D., et al. (2006). Vav1 acidic region tyrosine 174 is required for the formation of T cell receptor-induced microclusters and is essential in T cell development and activation. J. Biol. Chem. *281*, 38257–38265.

Minor, W., Cymborowski, M., Otwinowski, Z., and Chruszcz, M. (2006). HKL-3000: the integration of data reduction and structure solution–from diffraction images to an initial model in minutes. Acta Crystallogr. D Biol. Crystallogr. *62*, 859–866.

Moarefi, I., LaFevre-Bernt, M., Sicheri, F., Huse, M., Lee, C.H., Kuriyan, J., and Miller, W.T. (1997). Activation of the Src-family tyrosine kinase Hck by SH3 domain displacement. Nature *385*, 650–653.

Morris, R.J., Zwart, P.H., Cohen, S., Fernandez, F.J., Kakaris, M., Kirillova, O., Vonrhein, C., Perrakis, A., and Lamzin, V.S. (2004). Breaking good resolutions with ARP/wARP. J. Synchrotron Radiat. *11*, 56–59.

Otwinowski, Z. (1991). Isomorphous Replacement and Anomalous Scattering Proceedings of CCP4 Study Weekend, W. Wolf, P.R. Evans, and A.G.W. Leslie, eds. (Warrington, UK), pp. 80–86.

Prehoda, K.E., Scott, J.A., Mullins, R.D., and Lim, W.A. (2000). Integration of multiple signals through cooperative regulation of the N-WASP-Arp2/3 complex. Science *290*, 801–806.

Rapley, J., Tybulewicz, V.L., and Rittinger, K. (2008). Crucial structural role for the PH and C1 domains of the Vav1 exchange factor. EMBO Rep. *9*, 655–661.

Sauzeau, V., Sevilla, M.A., Rivas-Elena, J.V., de Alava, E., Montero, M.J., Lopez-Novoa, J.M., and Bustelo, X.R. (2006). Vav3 proto-oncogene deficiency leads to sympathetic hyperactivity and cardiovascular dysfunction. Nat. Med. *12*, 841–845.

Schindler, T., Bornmann, W., Pellicena, P., Miller, W.T., Clarkson, B., and Kuriyan, J. (2000). Structural mechanism for STI-571 inhibition of abelson tyrosine kinase. Science *289*, 1938–1942.

Schneider, T.R., and Sheldrick, G.M. (2002). Substructure solution with SHELXD. Acta Crystallogr. D Biol. Crystallogr. *58*, 1772–1779.

Sondermann, H., Soisson, S.M., Boykevisch, S., Yang, S.S., Bar-Sagi, D., and Kuriyan, J. (2004). Structural analysis of autoinhibition in the Ras activator Son of sevenless. Cell *119*, 393–405.

Tybulewicz, V.L. (2005). Vav-family proteins in T-cell signalling. Curr. Opin. Immunol. *17*, 267–274.

Utomo, A., Cullere, X., Glogauer, M., Swat, W., and Mayadas, T.N. (2006). Vav proteins in neutrophils are required for FcgammaR-mediated signaling to Rac GTPases and nicotinamide adenine dinucleotide phosphate oxidase component p40(phox). J. Immunol. *177*, 6388–6397.

Vajpai, N., Strauss, A., Fendrich, G., Cowan-Jacob, S.W., Manley, P.W., Grzesiek, S., and Jahnke, W. (2008). Solution conformations and dynamics of ABL kinase-inhibitor complexes determined by NMR substantiate the different binding modes of imatinib/nilotinib and dasatinib. J. Biol. Chem. *283*, 18292–18302.

Vogtherr, M., Saxena, K., Hoelder, S., Grimme, S., Betz, M., Schieborr, U., Pescatore, B., Robin, M., Delarbre, L., Langer, T., et al. (2006). NMR characterization of kinase p38 dynamics in free and ligand-bound forms. Angew. Chem. Int. Ed. Engl. *45*, 993–997.

Yohe, M.E., Rossman, K., and Sondek, J. (2008). Role of the C-terminal SH3 domain and N-terminal tyrosine phosphorylation in regulation of Tim and related Dbl-family proteins. Biochemistry *47*, 6827–6839.

Young, M.A., Gonfloni, S., Superti-Furga, G., Roux, B., and Kuriyan, J. (2001). Dynamic coupling between the SH2 and SH3 domains of c-Src and Hck underlies their inactivation by C-terminal tyrosine phosphorylation. Cell *105*, 115–126.